Jurnal Penelitian Fisika dan Aplikasinya (JPFA) *Volume 10, Issue 01, June 2020*
p-ISSN: 2087-9946 DOI: 10.26740/jpfa.v10n1.p44-55
e-ISSN: 2477-1775 https://journal.unesa.ac.id/index.php/jpfa

Research Article

Identification of Source Mechanisms for the August 5 2018 M_w 6.9 and the August 9 2018 M_w 7.0 Lombok Earthquakes

Ramadhan Priadi [1,a,*], Yusuf Hadi Perdana [1,b], Angga Wijaya [1,c], and Iman Suardi [1,2,d]

[1] Badan Meteorologi Klimatologi dan Geofisika
Jalan Angkasa I No.2 Kemayoran, Jakarta Pusat 10720, Indonesia
[2] Sekolah Tinggi Meteorologi Klimatologi dan Geofisika
Jalan Perhubungan 2, Tangerang Selatan 15221, Indonesia

e-mail: [a] ramadhanpriadi6@gmail.com, [b] yusuf.perdana@bmkg.go.id, [c] wijayaangga29@gmail.com, dan [d] imansuardi@yahoo.com
* Corresponding Author

Abstract

A series of earthquakes with magnitudes ranging from 5.8 to 7.0 occurred in Lombok in the period of July to August 2018. Two events occurred consecutively, the M_w 6.9 on August 5, 2018 (11:46:38 UTC), and the M_w 7.0 on August 9, 2018 (14:56:28 UTC). Those phenomena are rare because earthquakes usually require a relatively long time to accumulate their energies before being released. Because of those events, so an explanation is needed to explain what happened at the source. In this context, this study aims to determine the relations between the events based on the asperity zone and the slip distributions. Modeling was performed using teleseismic data and seismic inversion of body waves at low frequencies. The result shows that the asperity zone of M_w 6.9 is at 0 km in a strike-direction and -18 km wide in a dip-direction with a maximum slip of 1.3 m, whereas, for the M_w 7.0 event, the asperity zone is at -36 km in the direction of the strike and -7 km in the direction of the dip. Both events have the asperity in the up-dip section with an upward slip distribution towards the up-dip. The slip distribution of the first event and the second one has a relationship because the M_w 6.9 earthquake slip leads to the M_w 7.0 earthquake fault plane. The relation is suspected to be due to the weakening of rock conditions and an enlargement that is limited by space and time during the earthquake. As a result, those two earthquakes are closely related to stress distribution, forming a new asperity zone.

Keywords: *slip distribution; asperity; focal mechanism*

Identifikasi Mekanisme Sumber Gempa Bumi Lombok M_w 6.9 dan M_w 7.0 pada 5 dan 9 Agustus 2018

Abstrak

Gempa bumi signifikan dengan magnitudo yang berkisar antara M 5,8 hingga 7,0 terjadi di Lombok pada periode Juli hingga Agustus 2018. Terdapat 2 kejadian gempa bumi yang terjadi secara beruntun yaitu M_w 6,9 tanggal 5 Agustus 2018 (11:46:38 UTC) dan M_w 7,0 tanggal 9 Agustus 2018 (14:56:28 UTC). Fenomena tersebut sangat jarang terjadi karena gempa bumi memerlukan waktu yang relatif lama untuk mengakumulasi energi sebelum dilepaskan. Karena hal tersebut sehingga diperlukan penjabaran untuk

menjelaskan apa yang terjadi di sumber. Tujuan penelitian ini adalah untuk mengetahui hubungan antara kedua gempa bumi berdasarkan sebaran zona asperity dan distribusi slip yang terjadi. Pemodelan dilakukan dengan menginversi gelombang badan teleseismik pada frekuensi rendah. Hasil pemodelan menunjukkan bahwa zona asperity gempa bumi M_w 6,9 berada di panjang 0 km pada arah strike dan lebar -18 km pada arah dip dengan slip maksimum sebesar 1,3 m. Sedangkan hasil pemodelan gempa bumi M_w 7,0 zona asperity berada di -36 km pada arah strike dan -7 km pada arah dip. Kedua gempa bumi memiliki asperity pada bagian up-dip dengan distribusi slip naik menuju up-dip. Dari distribusi slip gempa bumi pertama dan gempa bumi kedua memiliki hubungan karena slip gempa bumi M_w 6,9 mengarah ke bidang sesar gempa bumi M_w 7,0. Keterkaitan tersebut diduga karena kondisi batuan yang melemah dan penyesaran yang dibatasi oleh ruang dan waktu selama gempa bumi terjadi. Sehingga kedua gempa tersebut berkaitan erat karena stress yang terdistribusi membentuk zona asperity yang baru.
Kata Kunci: *distribusi slip; asperity; focal mechanism*

PACS: 91.30.P-; 91.30.Px

Article History: Received: November 14, 2019 Approved with minor revision: May 22, 2020
Accepted: June 29, 2020 Published: June 30, 2020

How to cite: Priadi R, et al. Identification of Source Mechanisms for the August 5 2018 $\mathbf{M_w}$6.9 and the August 9 2018 $\mathbf{M_w}$7.0 Lombok Earthquakes. *Jurnal Penelitian Fisika dan Aplikasinya (JPFA)*. 2020; 10(1): 44-55. DOI: https://doi.org/10.26740/jpfa.v10.n1.p44-55.

I. INTRODUCTION

Lombok is one of the areas with high seismic activity due to the existence of the meeting of Indo-Australian with the Eurasian plate in the south, also the Flores back-arc thrust fault in the north [1]. The Flores's back-arc thrust extends from the north of Bali to Sumbawa [2]. There are several destructive earthquakes with range magnitudes from 5.8 to 7.0 that occurred in July-August 2018. Two significant earthquake events almost consecutive were the Lombok earthquake at 6.9 on 5 August 2018 (11:46:38 UTC) and the 7.0 earthquake on 9 August 2018 (14:56:28 UTC). The data is obtained from the IRIS (Incorporated Research Institution for Seismology) page.

An earthquake with magnitudes around 7.0 rarely coincides unless the earthquake triggers contact with asperity [3]. Asperity is a zone in the fault plane which has the largest slip value [4]. The asperity zone describes a buffer zone, where energy is locked and accumulated before being released as an earthquake. Asperity occurs in areas with the fewest aftershock [5]. Based on the Lombok earthquake phenomena' uniqueness on 5 and 9 August 2018, this research conducted a source mechanism modeling to provide more detailed identification of how the earthquakes occurred in a row.

One method that can be used to identify the earthquake source processes is modeling the source mechanism. The source information is contained in seismic waves. [6] A seismology approach to the source mechanism is needed to determine the fault plane and the rupture process at the source [7].

Some similar research has been carried out. First, Kikuchi and Kanamori [8] performed teleseismic wave inversions using P, SH, SV, and PP wave phases simultaneously. The simultaneous inversion aims to calculate the response from the source. Then, a study conducted by Yamanaka and Kikuchi [5] about body wave inversion using teleseismic data obtained if an earthquake has a recurring cycle from a

previous earthquake. It is evidenced by the rupture process, value of asperity, and slip direction, assuming that the asperity occurs in the areas with the least aftershock [9]. Besides that, Kikuchi et al. [10] prove that the most significant number of slips and energy is not only always in the hypocenter position but also in the asperity zone. Characterization of the source mechanism using teleseismic waves can provide more complete information than using near-field waves [3]. Teleseismic wave inversion can be used to interpret asperity, slip distribution, and orientation in the fault plane [11]. From the orientation and distribution slip, initial stress can be determined so that the relationships between other earthquakes can be determined [12].

From those studies above, the source mechanism's determination will be challenging to analyze due to the differences in source and surface perception. Therefore, this study about orthogonal projections is carried out to project the source's data into the surface [13]. Projections with a precise fault plane determination can provide a more accurate interpretation of the energy released zone before the earthquake so that the connections between the earthquakes can be estimated. Based on these explanations, this study aimed to determine the relations between two significant earthquakes in Lombok based on the source mechanism data.

II. METHOD

This research used teleseismic waveform data of the Lombok earthquake at 6.9 on 5 August 2018 (11:46:38 UTC) and the 7.0 earthquake on 9 August 2018 (14:56:28 UTC). The waveform data was obtained from the IRIS. The data used at the inversion process is teleseismic body wave data in the range of from the source to the station [14]. Teleseismic wave inversion is intended to reduce a local noise. The noise with a high frequency will be attenuated during the wave propagation process from the source to the station so that an excellent low-frequency seismic wave data could be obtained [8].

Initial parameters such as strike, dip, and rake are needed in modeling the source mechanism [15]. These parameters are obtained from Global CMT modeling results, which can be accessed through https://www.globalcmt.org/. The Global CMT provides information on two nodal fields, fault plane, and auxiliary plane. Unfortunately, Global CMT data does not include information on which nodal plane are fault plane and auxiliary plane. Eventually, HC-plot was used to distinguish ambiguity between the fault plane and the auxiliary plane in this study [16].

HC-plot describes the distance of the hypocenter to the centroid. The picture shows the plotting position of the hypocenter (H) and the centroid value (C) (see Figure.1) [16]. The hypocenter's position is in the point where rupture occurs for the first time, whereas the centroid is an approach to the slip point that is dominated in the fault [17]. The HC-plot assumes a planar fracture plane so that the fault plane becomes the closets nodal plane to the hypocenter, while the farther nodal is the auxiliary plane [18].

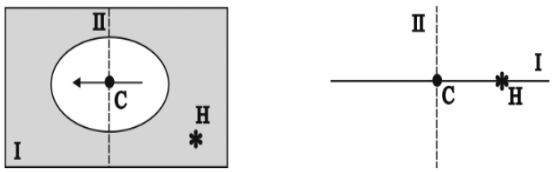

(a) **(b)**

Figure 1. (a) Schematic of the H-C Plot Method and (b) Schematic of the H-C Plot Method in Different Views but with the Same Conditions

Data inversion is done by deconvolution waves from the response instrument and the propagation effect from source to the station so that the initiation response form is received at the source [19]. The P, SH, SV, and PP body wave phases will

be inverted together; later, a multi-layer structure is used to calculate the source response. It is assumed that the source time function for a teleseismic earthquake resulted from the superposition of the ramp function [20].

The initiation wave at the source is a linear function of a combination of six independent elements from the basic components of the moment tensor, which is broken down into a source of multiple force pairs [21]. The basic components of moment tensor are represented by six independent elements of the matrix, as in equation 1.

$$M_1:\begin{bmatrix}0&1&0\\1&0&0\\0&0&0\end{bmatrix};\quad M_2:\begin{bmatrix}1&0&0\\0&-1&0\\0&0&0\end{bmatrix};$$
$$M_3:\begin{bmatrix}0&0&0\\0&0&1\\0&1&0\end{bmatrix};\quad M_4:\begin{bmatrix}0&0&1\\0&0&0\\1&0&0\end{bmatrix};$$
$$M_5:\begin{bmatrix}-1&0&0\\0&0&0\\0&0&1\end{bmatrix};\quad M_6:\begin{bmatrix}1&0&0\\0&1&0\\0&0&1\end{bmatrix}; \qquad (1)$$

The basic moment tensor matrix is obtained from seismic waves' inversion by matching the synthesis and the observation wave. [22] Firstly, prepared the Green function computation by calculating the source and the receiver function using the Haskell matrix. Then, the synthetic waveforms are obtained from source elements at each grid point [23]. The synthetic waveform that corresponds to moment tensor is formulated in the following equation [24]:

$$M_{ij} = \sum_{n=1}^{N_b} a_n M_n \qquad (2)$$

$$y_j(t;p) = \sum_{n=1}^{N_b} a_n w_{jm}(t;p) \qquad (3)$$

The synthesis signal is denoted as $y_j(t;p)$ with $w_{jm}(t;p)$, the Green's function that corresponds to the moment tensor element M_n. The parameter p indicates the time of onset and location of the slip distribution, while $x_j(t)$ shows the observational data recorded on several seismograms. The fault plane is assumed to have a temporal and spatial slip distribution in each direction [25], on each fault plane that is spatially extended by the following equation [26]:

$$\Delta\dot{u}_i(x,t) = \sum_{i=1}^{J} P^j \hat{u}_t^j(t)\phi^j(x) f^j(x,t) \qquad (4)$$

The unit vector representing the slip direction is denoted by $\hat{u}_t^j(t)$. The slip direction is always parallel to the fault plane and as a function of time [27]. The $\phi^j(x)$ is a spatial basis function and $f^j(x,t)$ is a function of the slip time. An integral is carried out in equation 4, for $t = \infty$ so that the final result of the slip distribution is summarized as [26]:

$$\Delta\dot{u}_i(x) = \sum_{i=1}^{J} P^j \hat{u}_t^j(t)\phi^j(x) \qquad (5)$$

$$\hat{u}_t^j = v_i^1 cos\hat{\theta}^j + v_i^2 sin\hat{\theta}^j \qquad (6)$$

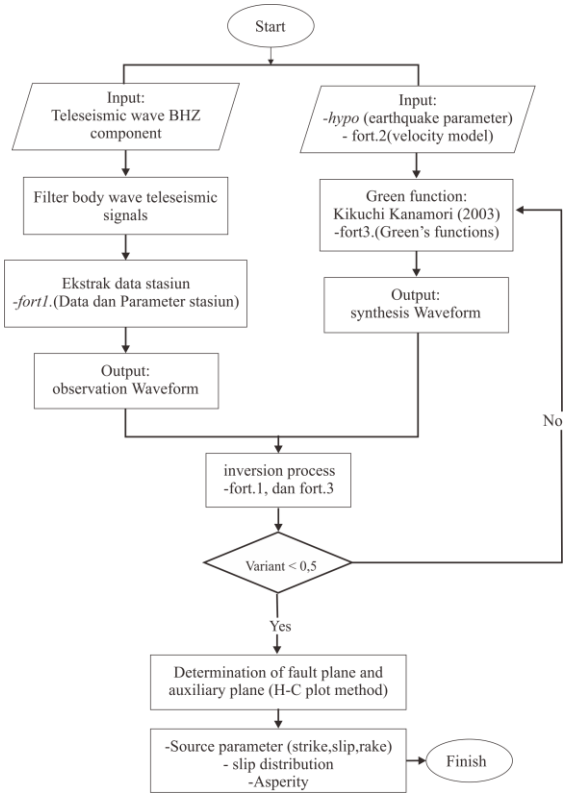

Figure 2. Flow Chart Data Acquisition and Teleseismic Body Wave Inversion Processing

Notation $\hat{u}_t^j$ shows the rake's direction in the final slip distribution, as described in equation 6. Two vector units which are perpendicular to the fault plane v^1 and v^2 are used to determine the final result of the slip distribution. The magnitude of the rake angle is denoted as $\hat{\theta}^j$ measured from v^1 and v^2.

Furthermore, the waveform data reconstruction is performed to obtain the slip distribution model and the asperity zone around the earthquake hypocenter [28]. Figure 2 shows a diagram of the teleseismic body wave inversion procedure. The input data is a filtered waveform. Extract the station data so that the waveform data used has already been correct first. Green's function is calculated based on earthquake parameters and the initial estimation of fracture plane orientation. Then the data will be converted to find out the observation wave and synthetic wave fitting. From these results, an analysis was conducted to determine the relationship between the two earthquakes based on the slip distribution.

III. RESULTS AND DISCUSSION

The parameters of the nodal plane 1 Lombok M_w 6.9 earthquake on August 5, 2018 (11:46:38 UTC) are known to strike at 92^0, dip 20^0, dan rake 94^0 while the nodal plane 2 is strike at 267^0, dip 70^0, and rake 89^0. Parameter of the nodal plane 1 Lombok M_w 7.0 earthquake on August 19, 2018 (14:56:28 UTC) known to strike at 96^0, dip 21^0, and rake 98^0 while the nodal plane 2 is strike at 267^0, dip 69^0, dan rake 87^0.

Figure 3 shows the results of the hypocenter plotting against centroids in the two Lombok earthquakes using HC-plot. The Lombok M_w 6.9 earthquake plot shows that the distance between nodal 1 to hypocenter is 5.50 km and the distance between nodal 2 to hypocenter is 6.92 km, with the distance between hypocenter to the centroid is 12.06 km. Based on these results, it was found that nodal 1 is a fault plane because it has a shorter distance than nodal 2.

Plotting of the Lombok M_w 7.0 earthquake shows that the distance between nodal 1 to the hypocenter is 4.04 km and the distance between nodal 2 to the hypocenter is 9.508 km with a distance between the hypocenter to the centroid is 23.66 km. According to these results, it was discovered that nodal 1 is a fault plane and nodal 2 is an auxiliary plane.

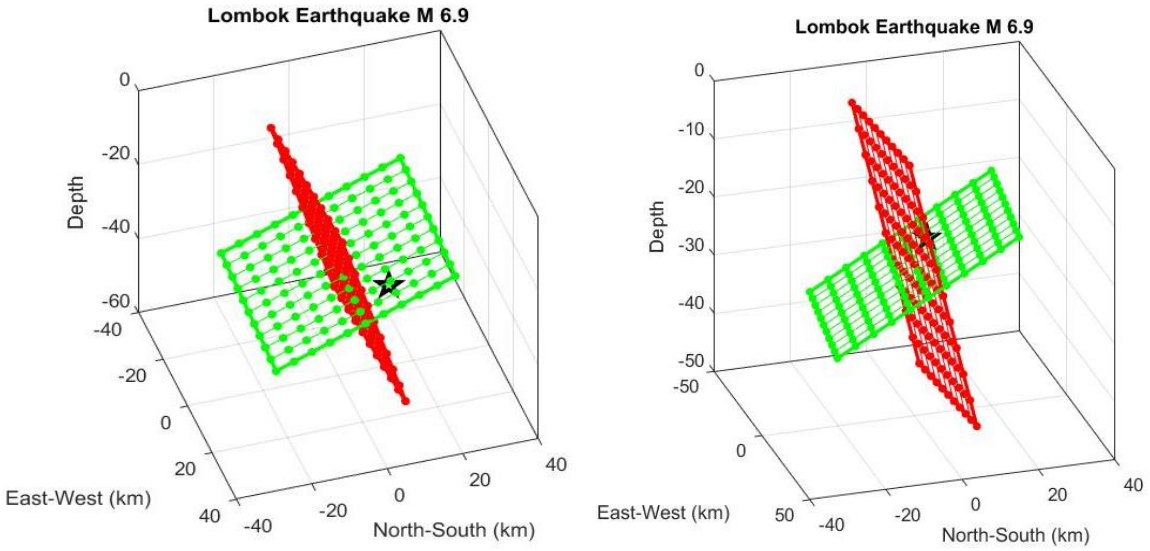

(a) **(b)**

Figure 3. Hypocenter and Centroid Plotting Results in an Earthquake: (a) M_w 6,9 (11:46:38 UTC) and (b) M_w 7,0 (14:56:28 UTC)

The nodal plane, which is selected as the fault plane, is used in the inversion process to produce slip distributions that correspond to tectonic conditions [29]. Figure 4 shows the results of the inversion and slip distribution of M_w 6.9 Lombok earthquake.

The iteration process on inversion updates of the source mechanism parameters to strike at 90^0, dip 20^0, and rake 88^0. A comparison between observation waves and synthesis waves results in a variant of 0.1462. Moment rate of inversion results obtained by M_0 0,430x10^{20} Nm, so that the renewal magnitude becomes M_w 7.02.

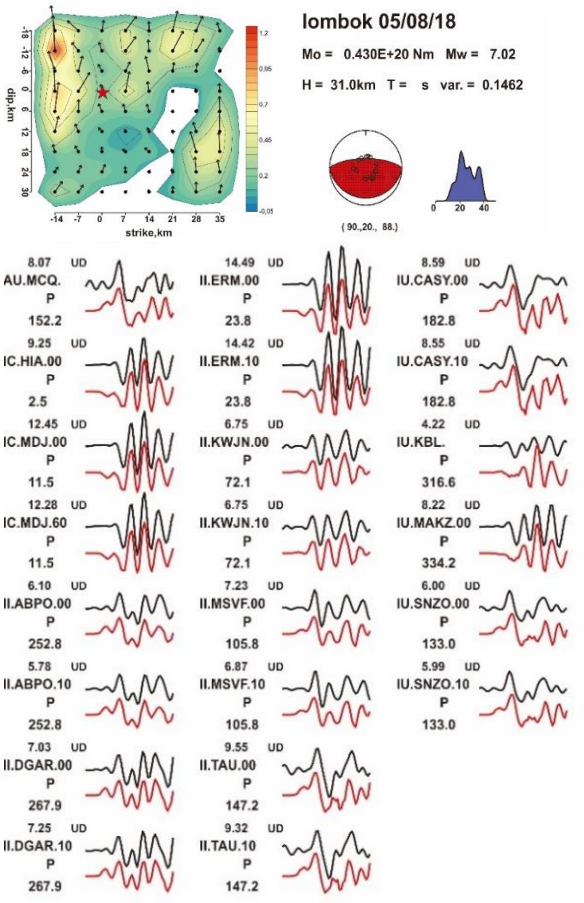

Figure 4. Results of Fault Plane Modeling and Wave Comparison in the Lombok Earthquake M_w 6,9 (11:46:38 UTC)

Teleseismic body wave inversion is a sensitive method for determining a slip area's depth using the depth phases (i.e., the -pP and -sP phases) [30]. The wide of the fault area from the inversion results is estimated to be 63 km long in strike direction and 60 km wide in dip direction. The fault area is divided into 8 × 9 sub-faults with dimensions of 7 km × 6 km for each subscale in the strike and dip direction. The fault plane is divided into sub-faults that have the same size. The size and the total number of sub-faults are chosen based on several considerations [31].

The iteration process in the inversion M_w 7.0 earthquake updates the source mechanism parameters to strike 96^0, dip 21^0, and rake 100^0 with a variant of 0.1349 between the observation wave and the synthesis wave. The synthetic signals are acquired from the determination of the finite fault source grid model [32]. Besides that, the use of the dip finite fault assumption also affects the inversion results [33]. The inversion moment rate is obtained at M_0 0.438x10^{20} Nm, so the magnitude update becomes M_w7.03.

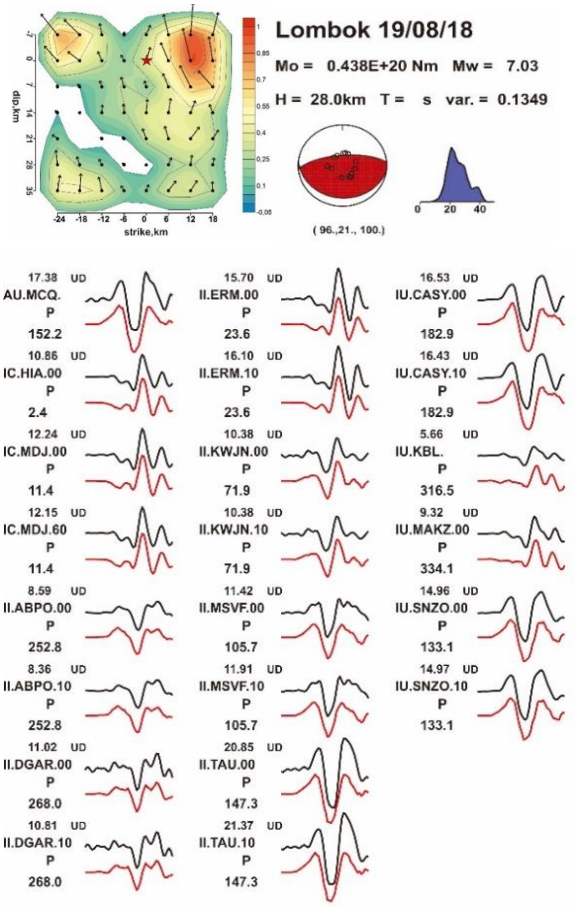

Figure 5. Results of Fault Plane Modeling and Wave Comparison in the Lombok Earthquake M_w 7,0 (14:56:28 UTC)

The type of fault is a reverse fault with a source duration of 40 s. The maximum slip which generated from the inversion process is 0.96 m. The dominant slip distribution leads almost perpendicular to the up-dip. Figure 5 shows the fault plane modeling and the wave ratio comparison in Lombok M_w 7.0 earthquake. The fault area's width from the inversion results is estimated to be 54 km long in the strike direction and 56 km in the dip direction. The fault area is divided into 8×7 sub-faults with dimensions of 6 km×7 km for each subscale in the strike and dip direction. The largest asperity zone is -12 km in strike direction and -0 km in dip direction.

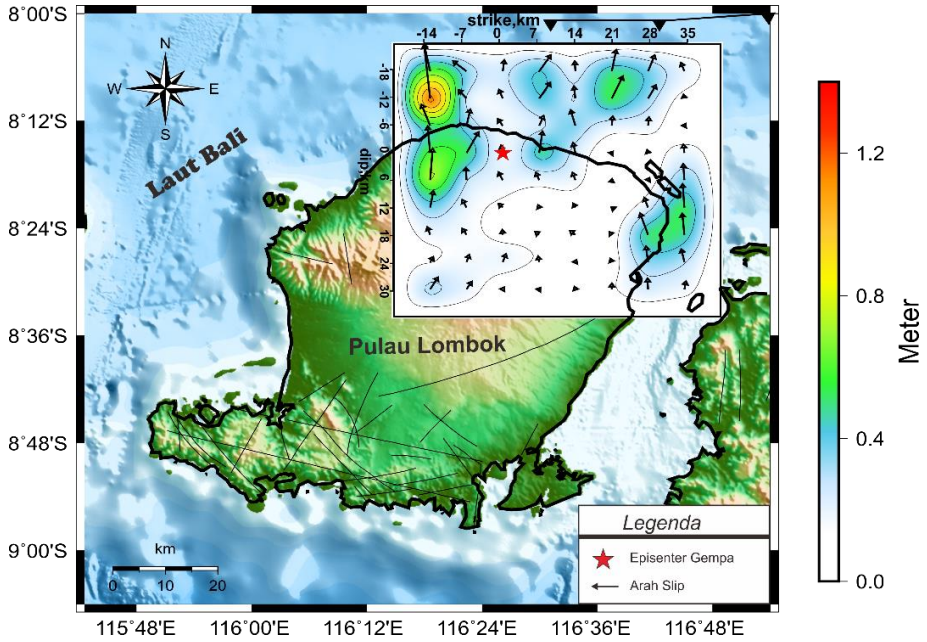

Figure 6. Map of Slip Distribution and Asperity Zones of the Lombok Earthquake M_w6,9 (11:46:38 UTC)

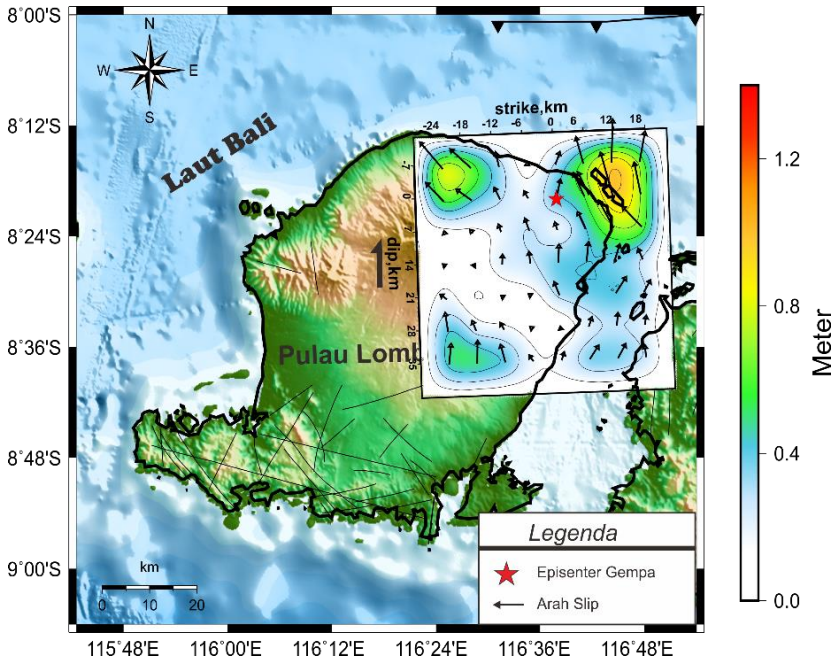

Figure 7. Map of Slip Distribution and Asperity Zones of the Lombok Earthquake M_w7,0 (11:46:38 UTC)

The type of fault is a reverse fault with a source duration of 46 seconds. An orthogonal projection is made to be able to certainty mapping the asperity zone in the Lombok region. Figure 6 shows a map of slip distribution and asperity zones from the orthogonal projection results in an M_w 6.9 earthquake. Based on the projection, it has resulted that the formed fault has a slight leftward direction. The largest asperity zone is in the up-dip position of the epicenter.

Figure 7 shows a map of slip distribution and asperity zones from orthogonal projection results in an M_w 7.0 earthquake. Based on the projections, the direction of the formed fault is almost perpendicular to the fault plane. The highest asperity zone is in the up-dip portion of the earthquake hypocenter while the maximum slip is in the highest asperity zone, west of the initial break. Asperity is half of the maximum slip of an earthquake [34]. This result is based on research by Kikuchi et al. [10] whose found that the earthquake strength and seismicity patterns are related to the distribution of asperity in each region.

Based on the research results from Yamanaka and Kikuchi [5], the Tokachi-Oki earthquake in 2003 was a repetition of the Tokachi-Oki earthquake in 1952. Viewed from the process that occurred was sourced based on the rupture process, asperity value, and slip direction with the assumption that the asperity arises in the region with the lowest aftershock. The results also show that the previous earthquake vector slip corresponds to the next earthquake. Similar to the results from previous studies, this study also showed the same pattern. Based on the modeling that has been done, the vector slips from the M_w 6.9 earthquake dominantly leads to the M_w 7.0 earthquake.

This fact reinforces the notion that the M_w 6.9 earthquake triggered an M_w 7.0 earthquake based on the dominant slip motion direction. According to Ratna et al. [35], it can be estimated that the energy released by the first event is the stress stored in the plane. So that one earthquake with another is the result of an extension of the previous earthquake energy accumulation.

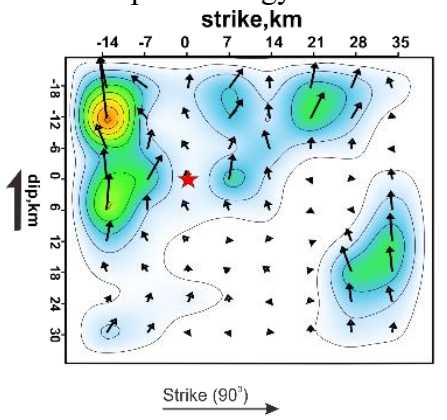

(a)

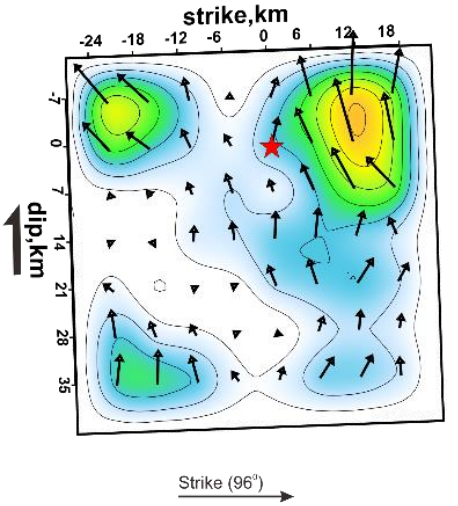

(b)

Figure 8. Fault Plane Modeling Results with the Corresponding Projection Strike Direction: (a) M_w 6,9 (11:46:38 UTC) and (b) M_w 7,0 (14:56:28 UTC)

Figure 8 shows the results of the modeling fault plane of each Lombok earthquake that has been projected and followed the strike's direction. It appears that the distribution of slip formed in the fault plane has a variety of directions but still has a dominant direction. The two planes' individual slip directions appeared differently, but both are dominantly pointing on the up-dip direction.

The modeling results show that the two earthquakes do not have a single asperity. More than one asperity is formed due to different rupture times for each asperity. The presence of slip release indicated the release of stress [36]. As a result, the Lombok earthquake has the size of a maximum magnitude that remains on an M 7 scale [37]. This result is presumably due to the brittle rock conditions and limited time and space enlargement [38].

Compared with the study by Sokos et al. [39], a single asperity takes 12 years to be formed again from the first earthquake released. Whereas in the Lombok earthquake, the event occurs close to a large magnitude, causing no single asperity to be formed [40]. In addition, based on research conducted by Zubaedah et al. [41], the earthquake that occurs is dominant in the northern region and close to the back-arc thrust but with the most activity in the shallow depth. This statement justifies the research results that show there is no single asperity because of the high seismicity in northern Lombok.

Referring to Kikuchi et al. research [10], which states that the distributed asperity cannot produce earthquakes with magnitudes greater than WAAA 7.0. This fact means that the earthquake that occurred in Lombok was very limited by space and time on the fault plane so that the release of energy occurred gradually and resulted in an independent earthquake [42]. The space limit is related to the fault area's width, while the time limit concerns the earthquake rupture time [43].

Estimating the processes that occur at the source required a lot of consideration and comparison parameters. Therefore, a lot of research is still needed to conduct in order to explain the phenomena. It is hoped that this research can be a reference in explaining the characteristics of significant earthquake source mechanisms that occur in Lombok.

IV. CONCLUSION

The northern region of Lombok experienced a weakening because it was no longer able to keep the accumulation of energy so that the earthquake was triggered by each other. Although the two earthquakes do not have a single asperity, the first earthquake slip distribution indicates that there is stress buildup during the period before the second earthquake. Identification of the source mechanism with the wave body inversion method in the future is expected to provide a reference in mapping earthquake hazard areas as disaster mitigation. A limitation of this study is that the resulting slip is a spatial result and cannot explain the temporal slip displacement.

ACKNOWLEDGMENT

Thanks to Kikuchi & Kanamori, IRIS (Incorporated Research Institution for Seismology), Global Centroid-Moment-Tensor, and BMKG (Badan Meteorologi Klimatologi dan Geofisika) who have helped in the preparation and processing of this paper.

REFERENCES

[1] Ibrahim G, Subardjo and Senjaya P. Tektonik Dan Mineral Di Indonesia. Jakarta: Puslitbang BMKG; 2010 .

[2] Silver EA, Breen NA, Prasetyo H and Hussong DM. Multibeam Study of the Flores Backarc Thrust Belt, Indonesia. *Journal of Geophysical Research: Solid Earth*. 1986; **91**(B3): 3489–3500. DOI: https://doi.org/10.1029/JB091iB03p03489.

[3] Yamanaka Y and Kikuchi M. Asperity Map along the Subduction Zone in Northeastern Japan Inferred from Regional Seismic Data. *Journal of Geophysical Research: Solid Earth*. 2004; **109**(B7). DOI: https://doi.org/10.1029/2003JB002683.

[4] Kikuchi M, Kanamori H and Satake K. Source Complexity of the 1988 Armenian Earthquake: Evidence for a Slow After-slip

Event. *Journal of Geophysical Research: Solid Earth*. 1993; **98**(B9): 15797–15808. DOI: https://doi.org/10.1029/93JB01568.

[5] Yamanaka Y and Kikuchi M. Source Process of the Recurrent Tokachi-Oki Earthquake on September 26, 2003, Inferred from Teleseismic Body Waves. *Earth, Planets and Space*. 2003; **55**(12): e21–e24. DOI: https://doi.org/10.1186/BF03352479.

[6] Dahm T and Kruger F. Moment Tensor Inversion and Moment Tensor Interpretation. Bormann, P. (Ed.), *New Manual of Seismological Observatory Practice. (NMSOP-2)*. Potsdam: Deutsches GeoForschungsZentrum GFZ; 2014: 1–37. DOI: https://doi.org/10.2312/GFZ.NMSOP-2_IS_3.9.

[7] Suardi I, Yagi Y, Widiyantoro S and Meilano I. *Analysis of Source Rupture Process of the September 2, 2009 Tasikmalaya Earthquake by using the Joint Inversion Method of Near Field and Teleseismic Data*. Bandung: Study Program of Earth Sciences, Institut Teknologi Bandung; 2013.

[8] Kikuchi M and Kanamori H. Inversion of Complex Body Waves-III. *Bulletin of the Seismological Society of America*. 1991; **81**(6): 2335–2350. Available from: https://pubs.geoscienceworld.org/ssa/bssa/article-abstract/81/6/2335/102472.

[9] Perfettini H, Frank WB, Marsan D and Bouchon M. A Model of Aftershock Migration Driven by Afterslip. *Geophysical Research Letters*. 2018; **45**(5): 2283–2293. DOI: https://doi.org/10.1002/2017GL076287.

[10] Kikuchi M, Nakamura M and Yoshikawa K. Source Rupture Processes of the 1944 Tonankai Earthquake and the 1945 Mikawa Earthquake Derived from Low-Gain Seismograms. *Earth, Planets and Space*. 2003; **55**: 159–172. DOI: https://doi.org/10.1186/BF03351745.

[11] Delouis B and Legrand D. Mw 7.8 Tarapaca Intermediate Depth Earthquake of 13 June 2005 (Northern Chile): Fault Plane Identification and Slip Distribution by Waveform Inversion. *Geophysical Research Letters*. 2007; **34**(1): L01304. DOI: https://doi.org/10.1029/2006GL028193.

[12] Liu C, Zheng Y, Xie Z and Xiong X. Rupture Features of the 2016 Mw 6.2 Norcia Earthquake and Its Possible Relationship with Strong Seismic Hazards. *Geophysical Research Letters*. 2017; **44**(3): 1320–1328. DOI: https://doi.org/10.1002/2016GL071958.

[13] Udias A. Development of Fault Plane Studies for the Mechanism of Earthquakes. *Observatory Seismology: A Centennial Symposium for the Berkeley Seismographic Stations First Edition*. California; 2018: 243–356.

[14] Yagi Y, Mikumo T, Pacheco J and Reyes G. Source Rupture Process of the Tecomán, Colima, Mexico Earthquake of 22 January 2003, Determined by Joint Inversion of Teleseismic Body-Wave and Near-Source Data. *Bulletin of the Seismological Society of America*. 2004; **94**(5): 1795–1807. DOI: https://doi.org/10.1785/012003095.

[15] Lay T and Wallace TC. *Modern Global Seismology*. San Diego: Acaddemic Press; 1995. Available from: https://www.elsevier.com/books/modern-global-seismology/lay/978-0-12-732870-6.

[16] Zahradnik J, Gallovic F, Sokos E, Serpetsidaki A, and Tseletis A. Quick Fault-Plane Identification by a Geometrical Method: Application to the Mw 6.2 Leonidio Earthquake, 6 January 2008, *Greece. Seismological Research Letters*. 2008; **79**(5): 653–662. DOI: https://doi.org/10.1785/gssrl.79.5.653.

[17] Kasmolan M, Santosa B, Lees J and Utama W. Earthquake Source Parameters at the Sumatran Fault Zone: Identification of the Activated Fault Plane. *Open Geosciences*. 2010; **2**(4): 455–474. DOI:

https://doi.org/10.2478/v10085-010-0016-5.

[18] Sianipar DSJ and Serhalawan YR. Pemodelan Mekanisme Sumber Gempa Bumi Ransiki 2012 Berkekuatan Mw 6,7. *JST (Jurnal Sains dan Teknologi)*. 2017; **6**(1): 148-157. DOI: http://dx.doi.org/10.23887/jst-undiksha.v6i1.9333.

[19] Clayton RW and Wiggins RA. Source Shape Estimation and Deconvolution of Teleseismic Bodywaves. *Geophysical Journal International*. 1976; **47**(1): 151–177. DOI: https://doi.org/10.1111/j.1365-246X.1976.tb01267.x.

[20] Kikuchi M and Kanamori H. Inversion of Complex Body Waves-II. *Physics of the Earth and Planetary Interiors*. 1986; **43**(3): 205–222. DOI: https://doi.org/10.1016/0031-9201(86)90048-8.

[21] Bormann P. New *Manual of Seismological Observatory Practice (NMSOP) Vol. 1-2*. Potsdam, Boulder: GeoForschungsZentrum Potsdam, IASPEI; 2002. Available from: https://gfzpublic.gfz-potsdam.de/pubman/item/item_229557.

[22] Song F and Toksöz MN. Full-Waveform Based Complete Moment Tensor Inversion and Source Parameter Estimation from Downhole Microseismic Data for Hydrofracture Monitoring. *Geophysics*. 2011; **76**(6): WC103–WC116. DOI: https://doi.org/10.1190/geo2011-0027.1.

[23] Meehan T. Evolution of the Propagator Matrix Method and Its Implementation in Seismology. *arXiv Geophysics*. 2018; 1-12. Available from: https://arxiv.org/abs/1801.04635.

[24] Kikuchi M and Kanamori H. Inversion of Complex Body Waves. *Bulletin of the Seismological Society of America*. 1982; **72**(2): 491–506. Available from: https://pubs.geoscienceworld.org/ssa/bssa/article-abstract/72/2/491/118251.

[25] Kikuchi M and Kanamori H. Rupture Process of the Kobe, Japan, Earthquake of Jan. 17, 1995, Determined from Teleseismic Body Waves. *Journal of Physics of the Earth*. 1996; **44**(5): 429–436. DOI: https://doi.org/10.4294/jpe1952.44.429.

[26] Ide S. 4.09-Slip Inversion. In Schubert, *Treatise on Geophysics, 2nd Edition.* Oxford: Elsevier; 2015: 215–241. Available from: https://www.elsevier.com/books/treatise-on-geophysics/schubert/978-0-444-53802-4.

[27] Gephart JW. Stress and the Direction of Slip on Fault Planes. *Tectonics*. 1990; **9**(4): 845–858. DOI: https://doi.org/10.1029/TC009i004p00845.

[28] Gusman AR, Satake K and Harada T. Rupture Process of the 2016 Wharton Basin Strike-slip Faulting Earthquake Estimated from Joint Inversion of Teleseismic and Tsunami Waveforms. *Geophysical Research Letters*. 2017; **44**(9): 4082–4089. DOI: https://doi.org/10.1002/2017GL073611.

[29] Shimizu K, Yagi Y, Okuwaki R and Fukahata Y. Development of an Inversion Method to Extract Information on Fault Geometry from Teleseismic Data. *Geophysical Journal International*. 2020; **220**(2): 1055–1065. DOI : https://doi.org/10.1093/gji/ggz496.

[30] Yoshimoto M and Yamanaka Y. Teleseismic Inversion of the 2004 Sumatra-Andaman Earthquake Rupture Process Using Complete Green's Functions. *Earth, Planets and Space*. 2014; **66**: 152. DOI: https://doi.org/10.1186/s40623-014-0152-4.

[31] Clayton BS, Hartzell SH, Moschetti MP and Minson SE. Finite-fault Bayesian Inversion of Teleseismic Body Waves. *Bulletin of the Seismological Society of America*. 2017; **107**(3): 1526–1544. DOI: https://doi.org/10.1785/0120160268.

[32] He X and Ni S. Rapid Rupture Directivity Determination of Moderate Dip-slip Earthquakes with Teleseismic Body Waves Assuming Reduced Finite Source Approximation. *Journal of Geophysical*

Research: Solid Earth. 2017; **122**(7): 5344–5368. DOI: https://doi.org/10.1002/2016JB013924.

[33] Yagi Y, Okuwaki R, Enescu B, Kasahara A, Miykawa A, and Otsubo M. Rupture Process of the 2016 Kumamoto Earthquake in Relation to the Thermal Structure around Aso Volcano. *Earth, Planets and Space*. 2016; **68**: 118. DOI: https://doi.org/10.1186/s40623-016-0492-3.

[34] El Fil H, Bobet A and Pyrak-Nolte LJ. Mechanical and Geophysical Monitoring of Slip Along Frictional Discontinuities. *Proceedings of 53rd US Rock Mechanics/Geomechanics Symposium, American Rock Mechanics Association*. New York; 2019: 23-26. Available from: https://www.onepetro.org/conference-paper/ARMA-2019-0449.

[35] Ratna PN, Gusman AR and Nugraha AD. Teleseismic Body Wave Inversion in Determining Rupture Process of Sumbawa Doublet Earthquake, November 25th, 2007. *IOP Conference Series: Earth and Environmental Science*. 2019; **318**: 012022. DOI: https://doi.org/10.1088/1755-1315/318/1/012022.

[36] Moschetti MP, Hartzell SH and Herrmann RB. Rupture Model of the M5. 8 Pawnee, Oklahoma, Earthquake From Regional and Teleseismic Waveforms. *Geophysical Research Letter*s. 2019; **46**(5): 2494–2502. DOI: https://doi.org/10.1029/2018GL081364.

[37] Wiemer S and Wyss M. Mapping the Frequency-magnitude Distribution in Asperities: An Improved Technique to Calculate Recurrence Times? *Journal of Geophysical Research: Solid Earth*. 1997; **102**(B7): 15115–15128. DOI: https://doi.org/10.1029/97JB00726.

[38] Chen X, Carpenter BM and Reches Z. Asperity Failure Control of Stick–Slip Along Brittle Faults. *Pure and Applied Geophysics*. 2020; **177**: 3225-3242. DOI: https://doi.org/10.1007/s00024-020-02434-y.

[39] Sokos E, Zahradnik J, Gallovic F, Serpetsidaki A, Plicka V, and Kiratzi A. Asperity Break after 12 Years: The Mw6. 4 2015 Lefkada (Greece) Earthquake. *Geophysical Research Letters*. 2016; **43**(12): 6137–6145. DOI: https://doi.org/10.1002/2016GL069427.

[40] Dublanchet P. Scaling and Variability of Interacting Repeating Earthquake Sequences Controlled by Asperity Density. *Geophysical Research Letters*. 2019; **46**(21): 11950–11958. DOI: https://doi.org/10.1029/2019GL084614.

[41] Zubaidah T, Korte M, Mandea M and Hamoudi M. New Insights into Regional Tectonics of the Sunda–Banda Arcs Region from Integrated Magnetic and Gravity Modelling. *Journal of Asian Earth Sciences*. 2014; **80**: 172–184. DOI: https://doi.org/10.1016/j.jseaes.2013.11.013.

[42] Ceferino L, Kiremidjian A and Deierlein G. Probabilistic Space-and Time-Interaction Modeling of Main-Shock Earthquake Rupture Occurrence. *Bulletin of the Seismological Society of America*; 2020. DOI: https://doi.org/10.1785/0120180220.

[43] Renou J and Vallée M. Observations of the Rupture Development Process from Source Time Functions. *Proceeding of 19th EGU General Assembly, EGU2017*. Vienna, Austria. 2017; **19**: 8968. Available from: https://ui.adsabs.harvard.edu/abs/2017EGUGA..19.8968R/abstract.